Power Electronics-Enabled Battery Management Systems for E-Mobility Applications

Energy Storage Systems

Frederik Holt Larsen

Power Electronics and Drives, PED4-1052, 2025-5

Master Thesis

AALBORG UNIVERSITY
STUDENT REPORT

AAU Energy
Aalborg University
9220 Aalborg Øst
Pontoppidanstræde 111
http://www.energy.aau.dk/

Title:
Power Electronics-Enabled Battery Management Systems for E-Mobility Applications

Theme:
Energy Storage Systems

Project Period:
Spring Semester 2025

Project Group:
PED4-1052

Participant(s):
Frederik Holt Larsen

Supervisor(s):
Arman Oshnoei
Hoda Sorouri

Page Numbers: 30

Date of Completion:
May 27, 2025

Abstract:

The adoption of electric vehicles has increased the demand for high performance and long lasting lithium-ion battery packs. This project investigates the development of a battery management system that uses active balancing through power electronic switches. The aim is to improve battery efficiency, safety, and longevity. The proposed method uses an artificial neural network to generate control signals for pulse width modulation of the switches. This enables dynamic management of both the state of charge and temperature across individual battery cells. A battery cell model is developed in MATLAB/Simulink, including state of charge estimation, open circuit voltage estimation, an equivalent circuit model, and a thermal model. These are then made into a modular battery pack model consisting of six cells. The artificial neural network control is trained to minimize deviations in state of charge and temperature, which it then uses to compute modulation signals for controlling the bypass switches. The simulation results show that effective balancing and convergence of both the state of charge and the temperature is done within 2500 seconds. A robustness test that included sensor noise up to $\pm 10\%$ is also made and it confirms the stability of the control. Furthermore, a virtual platform is used to validate the bypass method without involving real batteries. These results highlight the potential of using power electronic switches and a battery management system to improve battery performance, longevity, and efficiency in electric vehicle applications.

Summary

This master thesis presents the development of a power electronics-enabled battery management system for e-mobility applications. The work focuses on using artificial neural network control and active balancing by power electronic switches to improve the performance and lifetime of lithium-ion battery packs in electric vehicles.

The project includes a state of the art review which investigates state of charge estimation methods, battery modeling techniques, and cell balancing strategies. Based on this review, an equivalent circuit model is chosen due to its balance between accuracy and computational efficiency.

The battery modeling is done using MathWorks MATLAB/Simulink, where a battery cell model is built from four subsystems. These are state of charge estimation, open circuit voltage estimation, an equivalent circuit model, and a thermal model. These cell models are then connected in series to form a battery pack with switchable bypass paths. The switching is controlled using pulse width modulation signals obtained from the artificial neural network control.

Simulations show that the artificial neural network control achieves full state of charge and temperature balancing within 2500 seconds. The robustness of the system is also tested by adding noise to simulate sensor inaccuracies. The control remains effective, indicating high robustness to noise.

A virtual platform using digital signal processors and a Google Coral board is used to safely validate the system without real batteries. Here, the balancing method is tested which validated the effectiveness of the bypass method.

Although the artificial neural network control is not implemented on the virtual platform, the results support its potential as an efficient and intelligent control strategy. Future work includes deploying artificial neural network control on hardware, developing switching circuits, and testing on real battery cells.

Preface

The following software have been used during the writing of this report:

- Overleaf for text processing.
- MathWorks MATLAB/Simulink for calculations, modeling and simulations.
- Draw.io for figure composing.
- Microsoft 365 for data processing and sharing.

Aalborg University, May 27, 2025

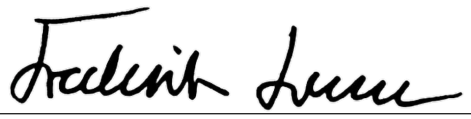

Frederik Holt Larsen
fhla19@student.aau.dk

Acronyms

ANN Artificial Neural Network.

BMS Battery Management Systems.

DDPG Deep Deterministic Policy Gradient.
DSP Digital Signal Processor.

ECM Equivalent Circuit Model.
EIM Electrochemical Impedance Models.
EM Electrochemical Models.
EVs Electric Vehicles.

FS-MPC Finite Set Model Predictive Control.

HIL Hardware in the Loop.

KNN K-Nearest Neighbor.

LiB Lithium-ion Battery.

MOSFET Metal-Oxide-Semiconductor Field-Effect Transistor.

OCV Open Circuit Voltage.

PWM Pulse Width Modulation.

SOC State of Charge.

Nomenclature

Units of measurement		
Symbol	**Explanation**	**Unit**
A	Surface area	m^2
C	capacitance	F
C_p	Specific heat capacity	$\frac{\mathrm{J}}{\mathrm{K \cdot kg}}$
E_c	Error signal	-
g	Activation function	-
H_j	Output function	-
h	Heat transfer coefficient	$\frac{\mathrm{W}}{\mathrm{m}^2 \cdot \mathrm{K}}$
I	Current	A
K	Iteration number	-
k_i	Control gain	-
L	Number of neurons	-
M	Number of neurons	-
m	Mass	kg
n	Number of cells	-
O_C	Output function	-
OCV	Open Circuit Voltage	V
Q	Heat generation rate	$\frac{\mathrm{W}}{\mathrm{m}^3}$
Q_{nom}	Nominal battery capacity	A h
R	Resistance	Ω
R_{th}	Thermal resistance	$\frac{\mathrm{K}}{\mathrm{W}}$
S	Switch	-
S'	Complementary switch	-
SOC	State of charge	%
SOC_{AV}	Average state of charge	%
T	Temperature	°C or K
T_A	Ambient temperature	°C or K
T_f	Temperature of fluid	K
t	Time	s
V	Voltage	V
V_{bat}	Battery voltage	V
V_g	Gate voltage	V
V_{OC}	Open circuit voltage	V
V_{out}	Output voltage	V
V_t	Terminal voltage	V
w_{ij}	Weighted neurons	-
w_{jc}	Weighted neurons	-
y_i	Input signal	-

Units of measurement		
Symbol	**Explanation**	**Unit**
Z	Impedance	Ω
Z_C	Capacitor impedance	Ω
Z_{eq}	Equivalent impedance	Ω
$Z_{eq,parallel}$	Equivalent parallel impedance	Ω
$Z_{eq.series}$	Equivalent series impedance	Ω
Z_R	Resistor impedance	Ω
η	Learning rate	-
δ	Error signal	-
ω	Angular frequency	rad/s
φ	Bias	-

List of Tables

3.1 Initial state of charge parameters. 11
3.2 Initial state of charge parameters. 12
3.3 Initial state of charge parameters. 13
3.4 Thermal model parameters. 13

List of Figures

2.1 Rint model.[11] 3
2.2 Thevenin model.[11] 4
2.3 Second order RC model.[11] 4
2.4 Discrete frequencies highlighted on a generic Nyquist plot, which is used to obtain the ECM parameters.[13] 5
2.5 Coupling relationship between the electrical and the thermal models.[13] 7
2.6 n series connected Smart Battery cells.[15] 8

3.1 Simplified battery cell model. 10
3.2 OCV-SOC curve. 11
3.3 Nyquist plot of 3.7 V/50 Ah NMC CALB prismatic cell. [15] 12
3.4 Battery pack model consisting of 6 battery cell models in series. 14

4.1 Electrical schematic of smart balancing system for a battery pack consisting of n serially connected cells. 15
4.2 Schematic of the ANN balancing control. 15
4.3 Generation of PWM signal. 17
4.4 Current. 18
4.5 Voltage. 18
4.6 SOC. 19
4.7 Temperature. 19
4.8 Current with noise. 20
4.9 SOC with noise. 21
4.10 Temperature with noise. 21

5.1 Virtual platform overview.[19] 22
5.2 Functions of all boards.[19] 23
5.3 Results of virtual platform test. 23

B.0.1 Overview of battery cell model in Simulink. II
B.1.1 SOC estimation in Simulink. II
B.3.1 ECM in Simulink. III
B.4.1 Thermal model in Simulink III

Contents

1 Introduction **1**
1.1 Problem Formulation . . . 2
1.1.1 Objectives . . . 2
1.1.2 Limitations . . . 2

2 State of the Art **3**
2.1 State of Charge Estimation Methods . . . 3
2.1.1 Equivalent Circuit Models . . . 3
2.1.2 Electrochemical Impedance Models . . . 4
2.1.3 Electrochemical Models . . . 4
2.2 Equivalent Circuit Modeling . . . 5
2.2.1 Frequency Selection for ECM Parameter Extraction . . . 5
2.2.2 Thevenin Modeling . . . 6
2.3 Thermal Modeling . . . 7
2.4 Cell Balancing Techniques . . . 8
2.5 Balancing Control of Switches . . . 9

3 Battery Modeling in Simulink **10**
3.1 Battery Cell Model . . . 10
3.1.1 State of Charge Estimation . . . 10
3.1.2 Open Circuit Voltage Estimation . . . 11
3.1.3 Equivalent Circuit Model Implementation . . . 12
3.1.4 Thermal Model . . . 13
3.2 Battery Pack Model . . . 14

4 Battery Management System **15**
4.1 Input Layer . . . 16
4.2 Hidden Layers . . . 16
4.3 Pulse Width Modulation . . . 17
4.4 Simulation Results . . . 18
4.5 Robustness Simulation . . . 20

5 Validation of Management System **22**

6 Discussion **25**
6.1 Use of Equivalent Circuit Model . . . 25
6.2 Simplified SOC Estimation . . . 25
6.3 Validation of ANN Control . . . 25
6.4 Ideal Switching . . . 25
6.5 Validation using Real Batteries . . . 26

7 Conclusion **27**

8 Future Work **28**

Bibliography **29**

A Simulink Model overview **I**

B Battery Cell Model **II**
B.1 SOC Estimation II
B.2 OCV Estimation II
B.3 ECM III
B.4 Thermal Model III

C ANN Control Function **IV**

1 Introduction

Globally, efforts are made with the aim of reducing carbon emissions. The European Union, among other regions, is committed to achieve net zero CO_2 emissions by 2050. This requires innovation in both power generation and transportation technologies. [1] One of the major contributors to CO_2 emissions is road transport, which accounts for 16% of cumulative emissions. In this sector, electrification is the primary strategy for decarbonizing road transport. [2] As a result, the number of Electric Vehicles (EVs) is increasing rapidly, leading to a growing demand for Lithium-ion Battery (LiB), which are widely used due to their lower weight, high energy density, superior output voltage, long lifespan, and safety. [3] [4] [5]

During the production of batteries, there are often challenges in achieving uniformity even within the same production line. This affects the EVs performance, since each battery cell will not be discharged evenly. To counteract this issue, a Battery Management Systems (BMS) is essential. It ensures vehicle safety, extends battery lifetime, minimizes costs, and maximizes driving range. [6] [7] As demand for LiB continues to rise, so does the need for advanced BMS solutions. [8] A typical BMS is responsible for performing key functions such as monitoring cell voltage and temperature, estimating the State of Charge (SOC), balancing cells to ensure uniform charge distribution, and providing isolation sensing and protection.

Recent advances in battery management research have focused on approaches that utilize machine learning, neural networks, and model estimations to improve precision and adaptability in balancing the cells. While conventional BMS strategies primarily focus on SOC balancing, recent studies also highlight the importance of temperature balancing in preventing accelerated degradation. Uneven heat distribution among cells leads to nonuniform aging and reduced overall battery capacity, which negatively impacts the longevity and performance of the battery pack. [9] [10]

1.1 Problem Formulation

The adoption of EVs has increased the demand for LiB. However, maintaining optimal battery performance over time is a major challenge due to imbalanced charge and discharge distribution among battery cells. This factor leads to reduced efficiency, safety risks, and shorter battery lifespans due to capacity fading and thermal instability. BMS operates to balance the cells, thus aiming to equalize the SOC and temperature across all cells in a battery pack. Conventional passive balancing techniques dissipate excess energy as heat, reducing overall efficiency. In contrast, active balancing methods redistribute energy among cells more efficiently but require complex power electronics and control algorithms. The effectiveness of a BMS depends on precise SOC estimation and efficient cell balancing strategies. Considering all this, the following problem statement is formulated:

How can a Battery Management System be developed, using power electronic switches and active balancing to improve battery performance, longevity, and efficiency in electric vehicle applications?

1.1.1 Objectives

In this project the main objectives are:

- Develop digital models for individual cells and the entire battery pack, including dynamic behaviors, cell connections, and bypass switches.
- Design a BMS that uses balancing strategies for both SOC and temperature.
- Validate the BMS method using Hardware in the Loop (HIL) testing.

1.1.2 Limitations

The project has the following limitations:

- The study focuses on the BMS. Therefore, an equivalent circuit model is used for SOC estimations. While it is efficient, it does not account for electrochemical degradation in the battery cell.
- The study does not explore alternative balancing architectures beyond using power electronic switches. while the investigated method might be efficiency, a comparison with other methods is not made.
- The study assumes ideal switching behavior when generating the PWM signals. It does not consider switching delays in turn ON and OFF or the energy losses.

2 State of the Art

A BMS is essential to ensure safe, efficient, and reliable operation of lithium ion battery packs. The BMS monitors key parameters such as voltage, temperature and SOC, while implementing a control strategy to enhance performance and extend battery lifespan. This section discusses the core functionalities of a BMS, including SOC estimation and cell balancing techniques, such as active balancing using power electronics and digital twin frameworks.

2.1 State of Charge Estimation Methods

SOC estimation determines the remaining charge within a battery relative to its full capacity. The accuracy of SOC estimation directly impacts the efficiency and reliability of an electric vehicle's power system. There are different approaches to estimate SOC, which can be categorized into three methods; Model-based, Ai-based and hybrid. The model-based methods estimate the SOC using mathematical models. AI-Based methods employ machine learning algorithms. Hybrid methods combine both model-based and ai-based methods. This project focuses on model-based methods. These methods require accurate battery cell modeling to develop a reliable BMS. Several modeling approaches exist, each with its own advantages and limitations. The three primary categories of battery models are Equivalent Circuit Model (ECM), Electrochemical Impedance Models (EIM) and Electrochemical Models (EM). [11]

2.1.1 Equivalent Circuit Models

The ECM is widely used due to their simplicity. These models represent battery behavior using electrical components such as resistors, capacitors, and voltage sources, which makes them computationally efficient for SOC estimation. Several ECM models can be used. Three commonly used models are described below.

The Rint model is seen in Figure 2.1. This is a basic ECM model which only uses an ideal voltage source and a resistor. This configuration allows for analysis of the dynamic behavior of the battery. The resistor value, R_0, varies with the SOC of the battery, the operating temperature, and if it is charging or discharging.

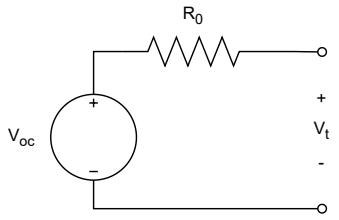

Figure 2.1 Rint model.[11]

The Thevenin model is seen in Figure 2.2. It uses an ideal voltage source and a resistor like the Rint model but adds a resistor and capacitor in parallel. This is also called a first-order RC model and it captures the transient response of a battery. It provides a balance between accuracy and computational efficiency.

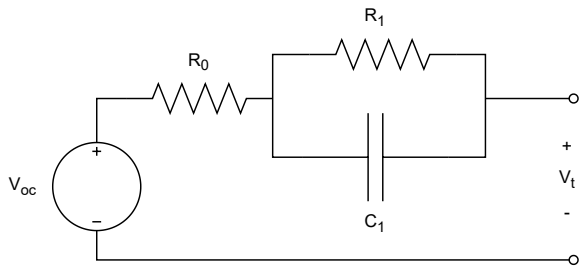

Figure 2.2 Thevenin model.[11]

The second order RC model is seen in Figure 2.3. It extends the Thevenin model by adding an extra RC pair to improve the representation of battery dynamics, particularly for more accurate transient response modeling. By doing so, it is more accurate but also adds more computational needs.

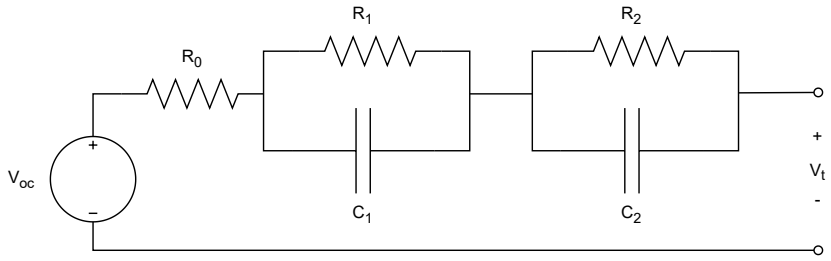

Figure 2.3 Second order RC model.[11]

Although the ECM provide simplicity, their accuracy depends on parameter identification, which can change due to aging, temperature variations, and operating conditions. [11] [12] [13]

2.1.2 Electrochemical Impedance Models

The EIM is based on impedance spectroscopy techniques, which characterize battery performance by measuring impedance at different frequencies. These models provide highly accurate representations of battery behavior, including internal resistance, charge transfer effects, and diffusion processes. Despite their high precision, an EIM is complex and requires specialized hardware to perform the impedance measurements. This makes them impractical for the estimation of SOC in conventional BMS. They are often used in laboratory settings to validate and improve the parameters of ECM. [11]

2.1.3 Electrochemical Models

EM provide a more physics based approach to battery modeling by capturing the internal chemical and physical processes governing lithium-ion transport, reaction kinetics, and charge dynamics. These models are derived from fundamental electrochemical equations. Although

an EM offer high accuracy and detailed insights into battery behavior, they require more computational resources and are therefore impractical for BMS applications. However, they are valuable for research, battery design optimization, and degradation analysis. [11]

2.2 Equivalent Circuit Modeling

In summary of Section 2.1, a ECM is widely used in practical BMS implementations, such as EVs. This is due to their computational efficiency. EIM and EM are primarily used in diagnostic and research applications to improve the accuracy of battery modeling and prediction of performance. Thus, this project will focus on ECM. Among the elaborated models, the Thevenin model is commonly used in electric vehicle applications because of its balance between simplicity and accuracy in representing battery impedance characteristics.

The Thevenin model captures the impedance response of lithium-ion cells over a wide frequency range while maintaining a low parameter count. This model is preferred because it only uses three parameters: R_0, R_1 and C_1, which can be analytically evaluated using impedance measurements at three discrete frequencies. The parameters of ECM correspond to specific internal battery behaviors. The resistance R_0 represents the electrolyte resistance, R_1 accounts for the charge transfer resistance, C_1 represents the double layer capacitance modeling charge accumulation on the electrode surface.[12][13]

2.2.1 Frequency Selection for ECM Parameter Extraction

The accuracy of the ECM parameters is highly dependent on the selection of frequencies for the measurement of the impedance. Here, three frequency regions must be used. A high frequency is used to determine R_0. A low frequency is used to determine R_1. A mid frequency is used to determine C_1. These frequencies are seen in Figure 2.4

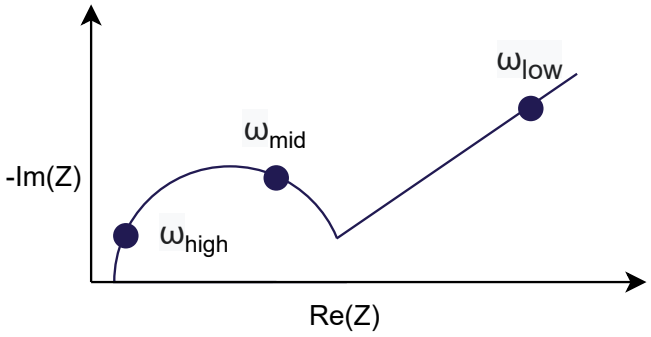

Figure 2.4 Discrete frequencies highlighted on a generic Nyquist plot, which is used to obtain the ECM parameters.[13]

2.2.2 Thevenin Modeling

To obtain the parameters of the Thevenin model, its electrical components are defined by their impedance, which is given by Equation 2.1 and Equation 2.2.

$$Z_R = R \tag{2.1}$$

$$Z_C = \frac{1}{j\omega C} \tag{2.2}$$

Using the relationship of impedance in series and in parallel, the equivalent impedance is determined, which is then isolated to obtain the parameters of the ECM. The general equations of impedance in series and in parallel are seen in Equation 2.3 and Equation 2.4, respectively.

$$Z_{eq,series} = Z_1 + Z_2 \tag{2.3}$$

$$\frac{1}{Z_{eq,parallel}} = \frac{1}{Z_1} + \frac{1}{Z_2} \tag{2.4}$$

The steps of which the equivalent impedance equations are formed and isolated to obtain the parameters of the ECM are now elaborated.

First R_0 is determined based on the chosen high frequency impedance. At high frequencies, the impedance is dominated by the ohmic resistance. Thus, the equivalent inductance equation is reduced to R_0. This is seen in Equation 2.5.

$$Z_{eq}(j\omega_{high}) \approx R_0 \tag{2.5}$$

Now that R_0 is known, R_1 is determined based on the chosen low frequency impedance. At lower frequencies, the total impedance incorporates both resistive and reactive parts, meaning the equivalent inductance reduces to Equation 2.6.

$$Z_{eq}(j\omega_{low}) \approx R_0 + R_1 \tag{2.6}$$

Extracting the real part of the impedance yields Equation 2.7.

$$Z_{low,real} = R_0 + R_1 \tag{2.7}$$

Last, to determine C_1, the chosen mid frequency impedance is used. At mid frequencies, the impedance is primarily influenced by capacitive effects. Thus, the equivalent inductance reflects a parallel RC circuit. This is seen in Equation 2.8.

$$Z_{eq}(j\omega_{mid}) \approx R_0 + \frac{R_1}{(1 + j\omega_{mid}R_1C_1)} \tag{2.8}$$

Separating this equation into its real and imaginary parts yields Equation 2.9 and Equation 2.10 respectively.

$$Z_{mid,real} = R_0 + \alpha \tag{2.9}$$

$$Z_{mid,imag} = \alpha\omega_{mid}R_1C_1 \tag{2.10}$$

Here, α is given by Equation 2.11.

$$\alpha = \frac{R_1}{1 + (\omega_{mid}R_1C_1)^2} \tag{2.11}$$

By using the real part of the impedance equation, α is determined. The capacitance C_1 is then determined by rearranging the imaginary part of the impedance. This is seen in Equation 2.12.

$$C_1 = \frac{Z_{mid,imag}}{\alpha \omega_{mid} R_1} \tag{2.12}$$

All parameters of the Thevenin model have now been defined.

2.3 Thermal Modeling

To effectively capture the thermal behavior of a battery, it is important to model the processes of heat generation, accumulation, and dissipation. An approach that can be used in control applications is the lumped-mass thermal model. An illustration of how this can be used in this control application is seen in Figure 2.5.

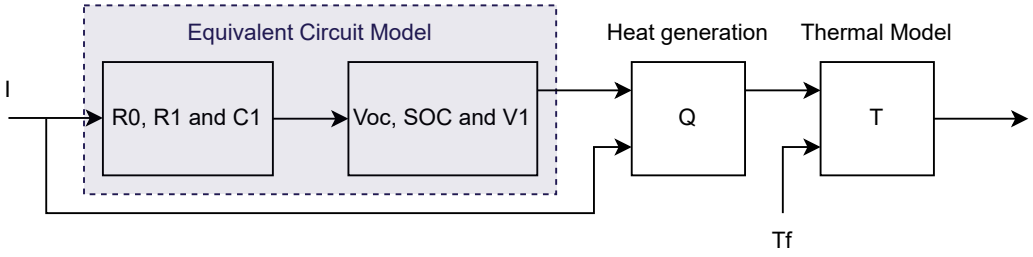

Figure 2.5 Coupling relationship between the electrical and the thermal models.[13]

The lumped-mass thermal model offers a balance between simplicity and computational efficiency. Here, the battery cell is represented as a single thermal mass, and its average temperature is used to characterize the cell's overall thermal condition. The thermal dynamics are described by Equation 2.13.

$$\frac{dT(t)}{dt} = \frac{hA}{mC_p} T(t) + \frac{1}{mC_p} Q(t) + \frac{hA}{mC_p} T_f(t) \tag{2.13}$$

In this equation, T is the bulk temperature of the cell, h is the heat transfer coefficient, A is the surface area of the cell, m is the mass of the cell, C_p is the specific heat capacity, Q is the heat generation rate, and T_f is the temperature of the surrounding fluid.

To determine the heat generation, a simplified model proposed by Bernardi et al. [14], is used. The model is shown in Equation 2.14.

$$Q(t) = I(t)[V_t(t) - V_{oc}(SOC)] + I(t)T(t) \cdot \frac{\partial V_{oc}}{\partial T}(SOC) \tag{2.14}$$

When implementing these equations in control applications there is a need for discrete-time thermal modeling. By using the zero-order hold method, Equation 2.13 and Equation 2.14 becomes Equation 2.15 and 2.16 respectively.

$$T(k+1) = T_k e^{\frac{hA}{mC_p}\Delta t} + (1 - e^{\frac{hA}{mC_p}\Delta t})(\frac{Q_k}{hA} + T_{f,k}) \tag{2.15}$$

$$Q(k) = I(k)^2 R_0 + I(k)V_{1,k} + I_k T_k \cdot \frac{\partial V_{oc}}{\partial T}(SOC_k) \tag{2.16}$$

2.4 Cell Balancing Techniques

non uniformity between cells lead to charge imbalances within a battery pack, reducing its overall efficiency and lifespan. Cell balancing techniques address this issue by redistributing energy among individual cells to ensure uniform charge levels. There are two primary types of cell balancing passive and active balancing. Passive balancing is simple, since it uses resistors, though this also means that energy is dissipated as heat. While being simple and having a low cost, this method is inefficient and contributes to thermal stress. Active balancing on the other hand, transfers energy between cells or modules by using power electronic components such as capacitors, inductors, or switches. This significantly improves the efficiency by reducing energy losses.[13]

Among the active balancing techniques, the one that utilizes power electronic switches is especially interesting due to its high potential.[15] This active balancing technique uses switches to insert or bypass battery cells in the battery pack allowing for precise control over SOC and temperature distribution. The technique is illustrated in Figure 2.6

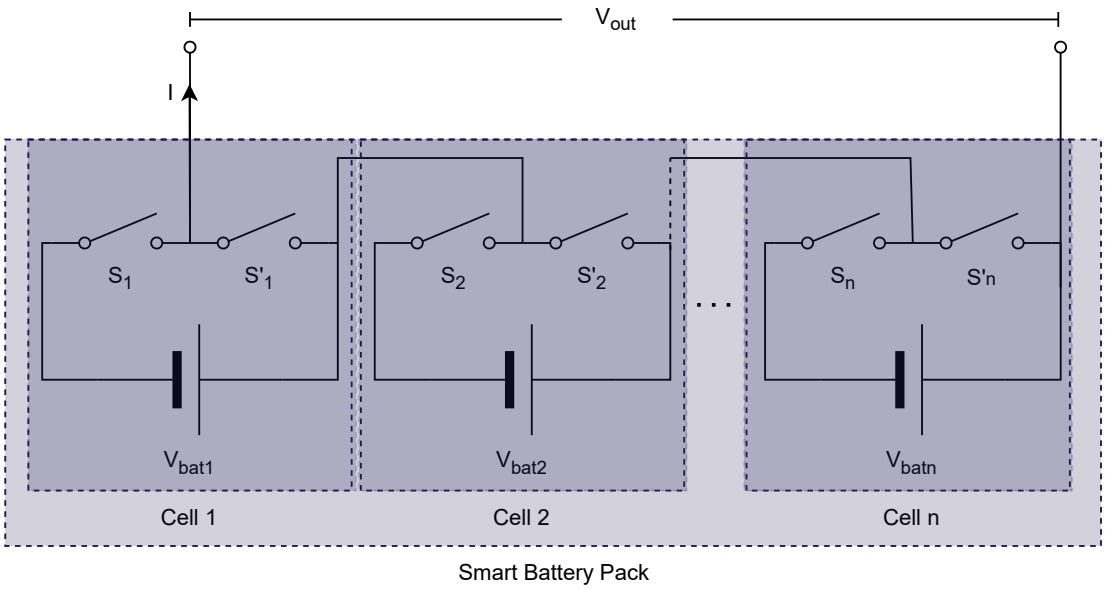

Figure 2.6 n series connected Smart Battery cells.[15]

The switches are configured in a half-bridge circuit in parallel to each cell. This results in two states for each cell. When the left switch is ON, the cell is inserted into the pack, while when the complementary switch to the right is ON, it will bypass the cell from the pack. This control mechanism ensures balanced SOC and temperature levels while extending the overall battery lifespan. [11][15]

2.5 Balancing Control of Switches

In Section 2.4 the concept of utilizing switches for active balancing is introduced. There are different methods to control the switching behavior in order to achieve a smart balancing structure. These methods are important since they allow efficient cell balancing and thus improves the energy efficiency. The methods investigated in this project are Finite Set Model Predictive Control (FS-MPC), Artificial Neural Network (ANN) and Deep Deterministic Policy Gradient (DDPG).

FS-MPC is a control approach that applies predictive models of battery dynamics to determine the optimal sequence of switch positions over a finite horizon. It uses a cost function in which it minimizes deviations. It then selects the optimal control input for the next time step. [16]

ANN control are particularly effective in handling nonlinearities and uncertainties in battery behavior. It uses a neural network to generate adaptive Pulse Width Modulation (PWM) control signals for the switches. This enables dynamic balancing across all cells. It also provides robustness against measurement noise and aging effects.[17].

DDPG is a reinforcement learning method capable of learning continuous control policies. A DDPG does not require a battery model because it learns optimal switching strategies through trial and error interactions with a simulation. Although DDPG achieves high performance in terms of balancing precision and adaptability, it requires substantial training time and computational resources.[18]

3 Battery Modeling in Simulink

The modeling of the battery is fundamental for the development, testing, and validation of a BMS. In this chapter, the process of implementing a lithium-ion battery model in MATLAB/Simulink is presented. The objective is to create a simulation that resembles the dynamic behavior of the battery under various SOC conditions, enabling the design and evaluation of control algorithms. This chapter, is divided into two sections. modeling of the individual cell and battery pack configuration. The first section focuses on making a battery cell model. The second section explains how individual cell models are connected to form a complete battery pack model.

3.1 Battery Cell Model

The modeled battery cells in this project are 3.7 V/50 Ah NMC CALB prismatic cells. The battery cell model consist of four subsystems. These subsystems are SOC estimation, Open Circuit Voltage (OCV) estimation, ECM, and a thermal model. Each of these subsystems is responsible for modeling the specific parameters needed to capture the dynamic behavior of the battery cell. A simplified illustration of how these are connected is seen in Figure 3.1. A print of the actual Simulink model is seen in Appendix B.

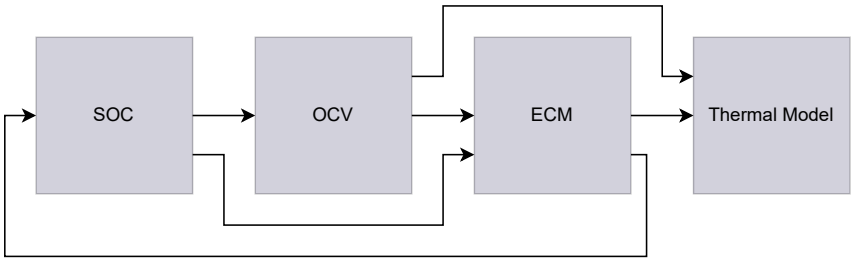

Figure 3.1 Simplified battery cell model.

The SOC subsystem estimates the SOC over time based on an initial SOC, current flow, and battery capacity. The OCV subsystem uses the SOC to determine the OCV, representing the steady-state voltage of the battery when the cell is bypassed. The ECM subsystem uses the SOC, OCV and a load dependent current to determine the voltage and current of the cell depending on if it is inline or bypassed. Lastly, the thermal model uses the voltage and current of the ECM to simulate the heat generation and dissipation in the cell. Each of these subsystems is explained in more detail in separate subsections.

3.1.1 State of Charge Estimation

The estimation of SOC is done by using Coulomb counting method. This method is commonly used due to its simplicity. It relies on current, capacity of the cell and an initial SOC value. Although this method is easily applicable it assumes that the current is accurate and that the capacity remains constant over time. The initial state of the battery is manually selected to

introduce an imbalance between cells, allowing the active balancing algorithm to be tested. The selected initial SOC values is seen in Table 3.1.

Table 3.1 Initial state of charge parameters.

Parameter	Value
Cell 1	1.00
Cell 2	0.95
Cell 3	0.90
Cell 4	0.85
Cell 5	0.80
Cell 6	0.75

The Coulomb counting method continuously updates the SOC based on the current flow. The SOC at any time t is calculated using Equation 3.1

$$SOC(t) = SOC_0 - \frac{1}{Q_{nom}} \cdot \int_{t_0}^{t} I(t)dt \tag{3.1}$$

Where $SOC(t)$ is the state of charge at time t. SOC_0 is the initial state. Q is the nominal capacity of the battery cell. $I(t)$ is the current at time t, obtained from the ECM. A print of this imputed in Simulink is seen in Appendix B.1.

3.1.2 Open Circuit Voltage Estimation

When a battery cell is bypassed, there is still an electrical potential between the positive and negative terminals. This voltage is defined as the OCV. It is important to include this parameter since it models the steady-state behavior of the cell when bypassed and thus result in a more precise SOC estimation. To determine the OCV of the chosen cell, it is tested in the laboratory. The battery cell is charged and discharged at a very low current, which is assumed to be negligible. This ensures that the measured voltage closely approximates the true OCV corresponding to each SOC level. The resulting curve is seen in Figure 3.2.

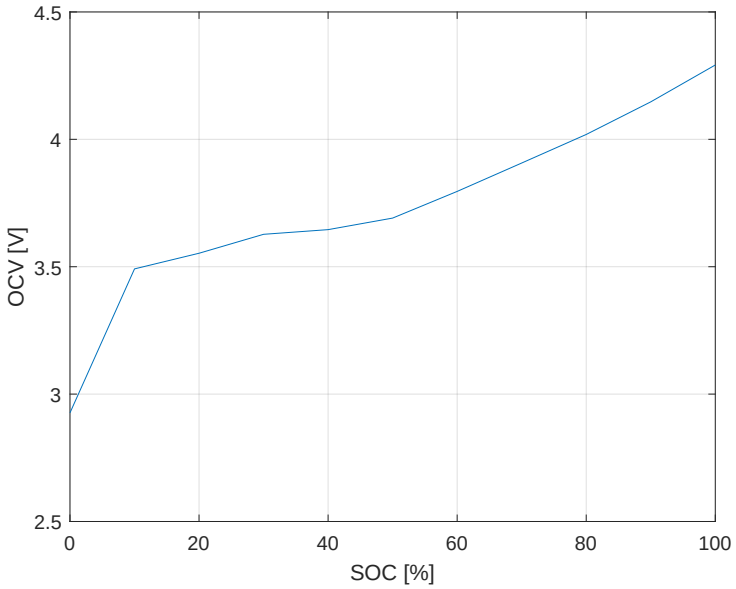

Figure 3.2 OCV-SOC curve.

By curve fitting the experimental data, the relationship between the SOC and the OCV is expressed by a nonlinear function, which is shown in Equation 3.2.

$$OCV = p_1 \cdot x^9 + p_2 \cdot x^8 + p_3 \cdot x^7 + p_4 \cdot x^6 + p_5 \cdot x^5 + p_6 \cdot x^4 + p_7 \cdot x^3 + p_8 \cdot x^2 + p_9 \cdot x + p_{10} \tag{3.2}$$

Where x is the SOC. The parameters of the fitted OCV function are summarized in Table 3.2.

Table 3.2 Initial state of charge parameters.

Parameter	Value	Unit
p_1	$2.18e^3$	V
p_2	$-1.06e4$	V
p_3	$2.18e^4$	V
p_4	$-2.47e^4$	V
p_5	$1.67e^4$	V
p_6	$-6.92e^3$	V
p_7	$1.72e^3$	V
p_8	$-2.43e^2$	V
p_9	18.2	V
p_{10}	2.93	V

These values are used as inputs to the battery cell model for better SOC estimation. The Matlab code is shown in Appendix B.2.

3.1.3 Equivalent Circuit Model Implementation

In Section 2.2 it is decided to use the Thevenin model. To obtain the parameters experimental inductance tests where made which is detailed in [15]. In short electrochemical impedance spectroscopy is used to characterize the resistances and capacitance of the selected 3.7 V/50 Ah NMC CALB prismatic cell. The setup consists of a battery tester, a thermal chamber and a host PC for data gathering. Multiple experiments are carried out. First the SOC is adjusted to different values while keeping the temperature constant. After which the temperature is changed while maintaining the same SOC. Each measured impedance spectrum is represented by a Nyquist plot. These are seen in Figure 3.3.

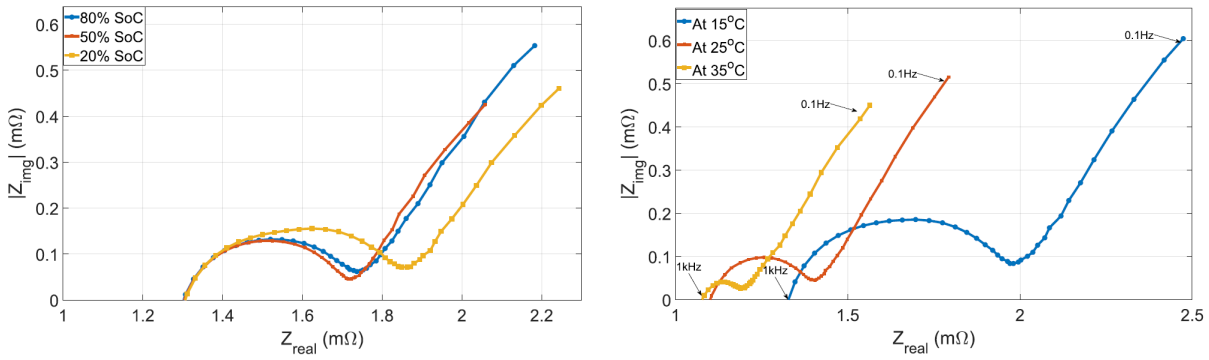

(a) Nyquist plot at different SOCs. **(b)** Nyquist plot at different temperatures.

Figure 3.3 Nyquist plot of 3.7 V/50 Ah NMC CALB prismatic cell. [15]

Based on the average of these inductance measurement, the ECM parameters is then calculated by the equations given in Section 2.2.2. The extracted parameters are summarized into Table 3.3.

Table 3.3 Initial state of charge parameters.

Parameter	Value	Unit
R_0	$1.47e^{-3}$	Ω
R_1	$0.159e^{-3}$	Ω
C_1	5.08	F

These parameters are assigned to their respective electrical components in the ECM model in Simulink. In addition to R_0, R_1 and C_1, the model also include a controlled current source and controlled voltage source. The current source provides the rated current when the cell is inline while the voltage source represents the OCV when the cell is bypassed. A printed overview of the ECM in Simulink is shown in Appendix B.3.

3.1.4 Thermal Model

To simulate the heat generation and dissipation in the battery cell, a thermal model is implemented using the Simscape toolbox in Simulink. The thermal model estimates the temperature of the battery cell based on power dissipation and thermal properties. The model uses the current and voltage from the ECM and converts it into heat. This is done using the mass m, specific heat capacity C_p, and thermal resistance R_{th} of the 3.7 V/50 Ah NMC CALB prismatic cell. Each of these properties is seen in Table 3.4.

Table 3.4 Thermal model parameters.

Parameter	Value	Unit
m	0.076	kg
C_p	1100	$\frac{\text{J}}{\text{K}\cdot\text{kg}}$
R_{th}	2.5	$\frac{\text{K}}{\text{W}}$

The output of the thermal model is the battery cell temperature, which dynamically updates based on operating conditions. By adding this thermal model, the entire system can evaluate the impact of current loads on temperature, which is then controllable by balancing strategies. A printed overview of the thermal model in Simulink is shown in Appendix B.4.

3.2 Battery Pack Model

The battery pack model consist of six individual cell models connected in series. Each cell has the structure defined in Section 3.1. The pack is designed to share a fixed load, represented by a controlled current source. The structure of the Battery pack model is seen in Figure 3.4.

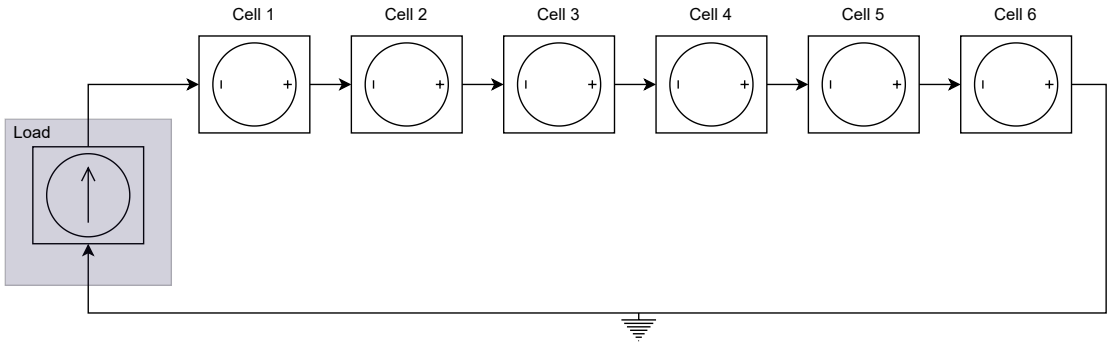

Figure 3.4 Battery pack model consisting of 6 battery cell models in series.

Each individual cell can be switched ON or OFF based on a binary control signal. The switching is later controlled by the BMS to enable balancing of SOC. If the cell is inline the current in the cell is equal to the fixed current load. When the cell is bypassed it still has a electrical potential equal to the OCV. The total voltage of the battery pack is the sum of all six cell voltages, meaning it changes depending on how many cells that are inline and bypassed. Since each cell has its own thermal model, the temperature of each cell is determined individually. This allows the BMS to regulate thermal conditions. It is done by comparing the temperature of each cell and bypassing them if the relative temperature is over a set level. This prevents one cell from overheating. In summary the developed battery pack model serves as the foundation for evaluating control strategies. Allowing testing, and validation of BMS.

4 Battery Management System

In Section 2.5 different methods of controlling the switches is proposed. Among them, ANN is selected due to its simplicity and ability to adapt to changes in the battery cells condition. The goal of implementing ANN is to minimize SOC and temperature deviations from an average or standard value. The output of ANN is modulation signals that are used to create PWM signals for switches, thus obtaining balancing control. A schematic of the entire system is seen in Figure 4.1. Whereas a more detailed schematic of the proposed ANN balancing control system is seen in Figure 4.2. Each part of this control system is explained further in separate sections.

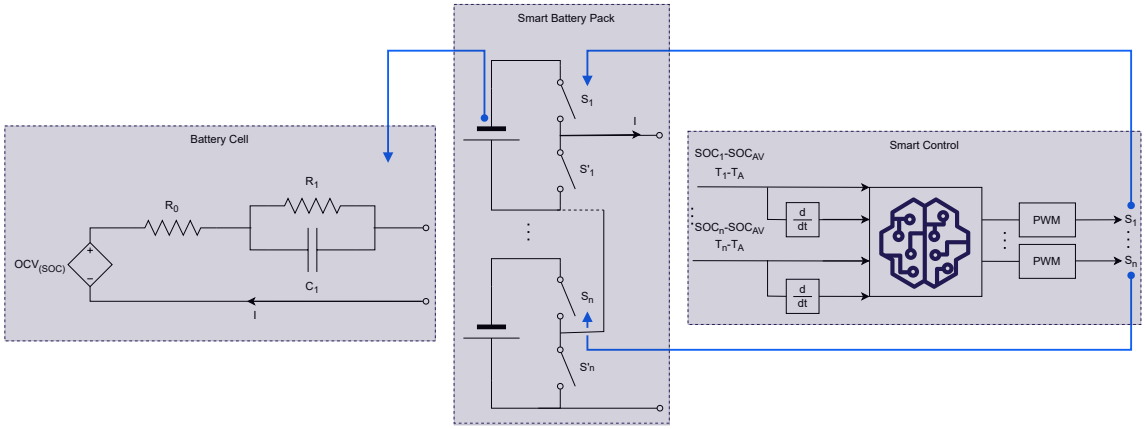

Figure 4.1 Electrical schematic of smart balancing system for a battery pack consisting of n serially connected cells.

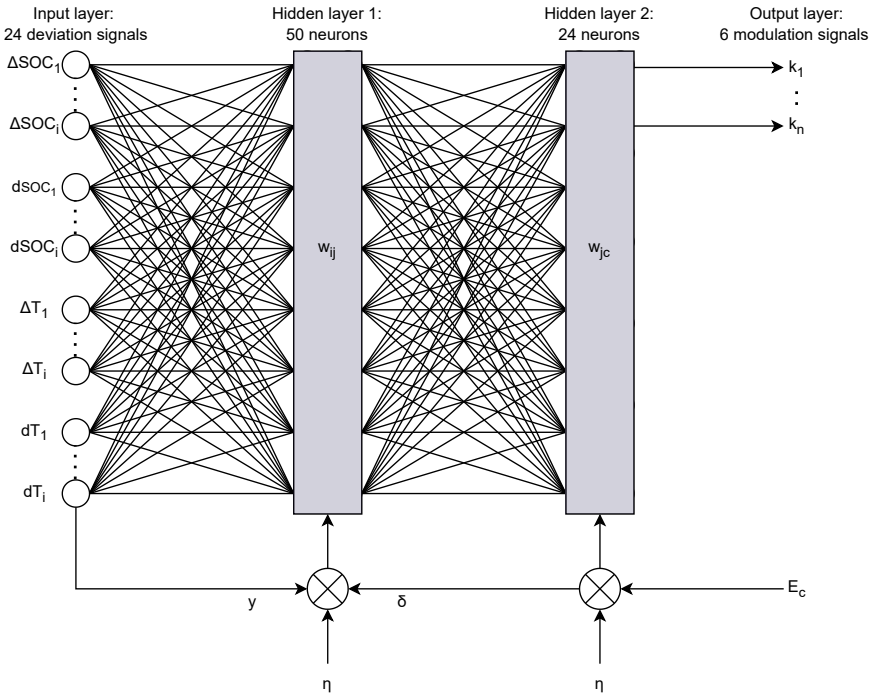

Figure 4.2 Schematic of the ANN balancing control.

4.1 Input Layer

To enable smart switching decisions, deviation input signals needs to be calculated. For controlling the SOC, the average SOC across all six battery cells is calculated. This is done in Equation 4.1.

$$SOC_{AV} = \frac{1}{n}\sum_{i=1}^{n} SOC_i, \quad \text{for} \quad i \in n \tag{4.1}$$

Here n is the number of cells and SOC_i is the SOC of each cell. The SOC of each cell are then compared to the average in order to determine the deviation for each cell. This is seen in Equation 4.2.

$$\Delta SOC_i = SOC_{AV} - SOC_i, \quad \text{for} \quad i = 1, 2, \ldots, n \tag{4.2}$$

For controlling the temperature, a fixed reference temperature of $25°C$ is used instead of an average. This temperature is chosen based on the ideal operating condition of lithium-ion cells. The temperature deviation is calculated by Equation 4.3.

$$\Delta T_i = 25°\text{C} - T_i \tag{4.3}$$

Additionally, To avoid large changes in the balancing control the rate of change is also considered. This is done by taken the derivative of both SOC and temperature deviations. This is seen in Equation 4.4.

$$dSOC_i = \frac{d\,\Delta SOC_i}{dt}, \quad dT_i = \frac{d\,\Delta T_i}{dt} \tag{4.4}$$

In total 24 input signals are calculated to form the input layer of the ANN control. The objective of the learning process is to reduce these deviations.

4.2 Hidden Layers

The implementation of ANN includes two hidden layers. Each layer uses processing units known as neurons. These neuron consists of weights, w, an activation function, $g(x)$, and a bias, φ. The output function of hidden layer 1 is H_j and is given by Equation 4.5.

$$H_j = g(\sum_{i=1}^{n} w_{ij} y_i + \varphi), \quad \text{for} \quad j = 1, 2, ..., L \tag{4.5}$$

Where L is the total number of neurons in the hidden layer. In hidden layer 1 50 neurons are used, each with its own weight. The weights are given by Equation 4.6.

$$w_{ij}(k+1) = w_{ij}(k) + \eta\delta y \quad \text{for} \quad i = 1, 2, ..., n, \quad j = 1, 2, ..., L \tag{4.6}$$

Here, w_{ij} is the weight at each iteration k. η is the learning rate, which determines how much the weights are adjusted at each iteration. δ is the error signal from the output layer. y is the input signal to the neural network. The activation function for this hidden layer is sigmoid which is given by Equation 4.7.

$$g(x) = \frac{1}{1 + e^{-x}} \tag{4.7}$$

This hidden layer does not include a bias and thus it is equal to zero.

Hidden layer 2 transforms the output of hidden layer 1 into a suitable number of outputs for the output layer, which should consist of one output for each cell. It uses H_j as a input signal and has the output function O_c, which is given by Equation 4.8.

$$O_c = \sum_{j=1}^{L} H_j w_{jc} + \varphi, \quad \text{for} \quad c = 1, 2, ..., M \tag{4.8}$$

Here, M is the number of neurons in the hidden layer. It uses 24 neurons with linear activation and no bias. The weights are given by Equation 4.9.

$$w_{jc}(k+1) = w_{jc}(k) + \eta H_j E_c \quad \text{for} \quad j = 1, 2, ..., L, \quad c = 1, 2, ..., M \tag{4.9}$$

Where E_c is the error signal including the deviations of SOC and temperature. From the output of hidden layer 2, selected neurons are combined to form six control gains, k_1 to k_6 each representing an individual cell. The expressions of these are listed below:

$$k_1 = 0.5 \cdot (0.9 \cdot O_c(2) - 0.2 \cdot O_c(3)) \tag{4.10}$$

$$k_2 = 0.5 \cdot (0.9 \cdot O_c(6) - 0.2 \cdot O_c(7)) \tag{4.11}$$

$$k_3 = 0.5 \cdot (0.9 \cdot O_c(10) - 0.2 \cdot O_c(11)) \tag{4.12}$$

$$k_4 = 0.5 \cdot (0.9 \cdot O_c(14) - 0.2 \cdot O_c(15)) \tag{4.13}$$

$$k_5 = 0.5 \cdot (0.9 \cdot O_c(18) - 0.2 \cdot O_c(19)) \tag{4.14}$$

$$k_6 = 0.5 \cdot (0.9 \cdot O_c(22) - 0.2 \cdot O_c(23)) \tag{4.15}$$

These gains will serve as modulation signals for PWM control of the switches. From these gains it is also seen that selected weights have been assigned, prioritizing SOC over temperature. The Matlab code for the ANN control is shown in Appendix C.

4.3 Pulse Width Modulation

To allow for the balancing of the switches, the control gains k_1 through k_6 are used as modulation signals in a PWM scheme. Each gain is compared to a sawtooth carrier waveform. When the gain exceeds the carrier signal, the corresponding switch is turned ON and the cell is inline. Otherwise, the cell is bypassed. An illustration of this is seen in Figure 4.3.

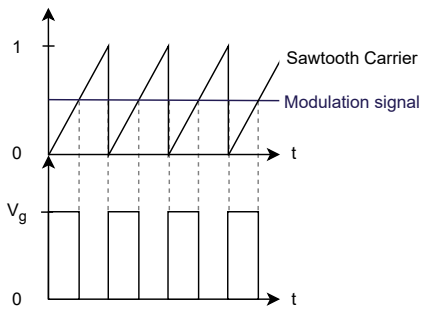

Figure 4.3 Generation of PWM signal.

This approach enables independent control of each cell, allowing some cells to be used more and others less, thus achieving balancing of both SOC and temperature.

4.4 Simulation Results

Simulations are conducted with the battery pack consisting of six 3.7 V/50 Ah NMC CALB prismatic cell models, each with the characteristics explained in Chapter 3. Here, it is also elaborated that each cell is given a different initial SOC. All cells have a uniform initial temperature of 25°C. A constant external current of 50 Amps is applied through the entire simulation. The results of the simulation are seen in Figure 4.4-4.7.

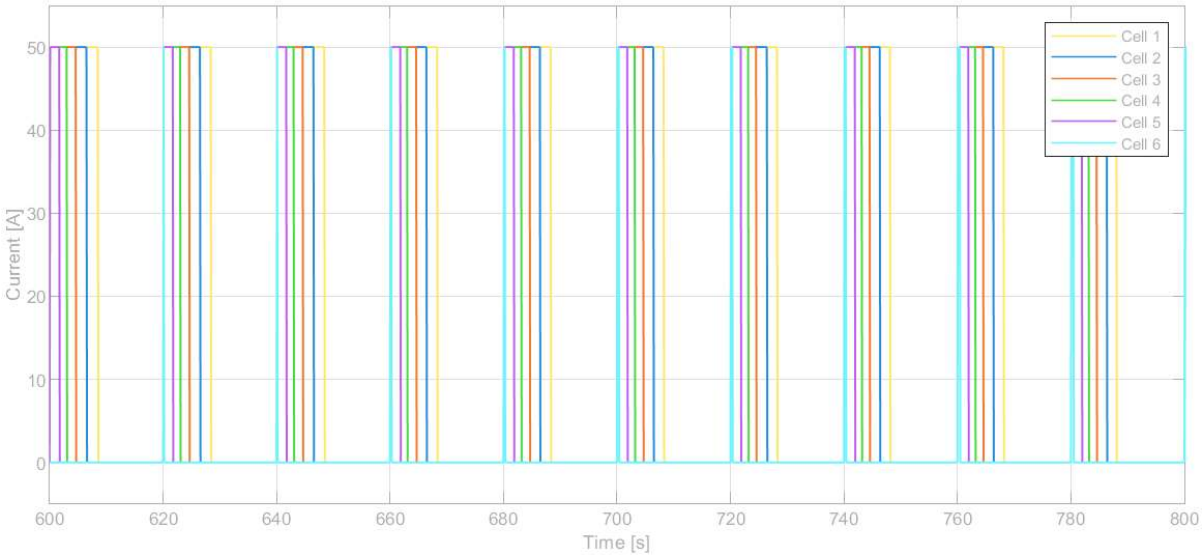

Figure 4.4 Current.

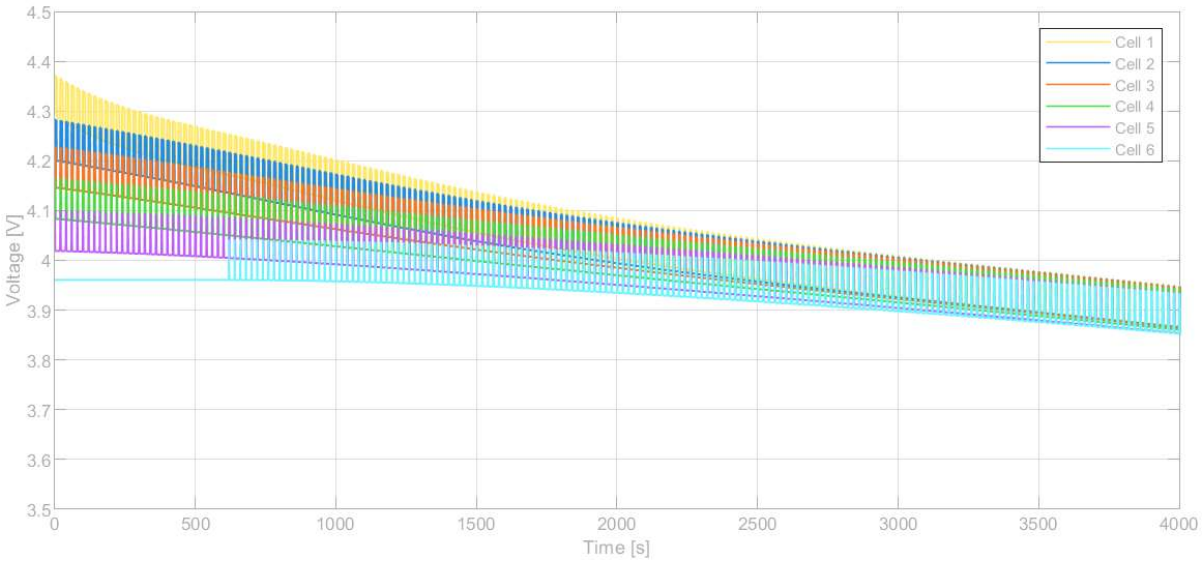

Figure 4.5 Voltage.

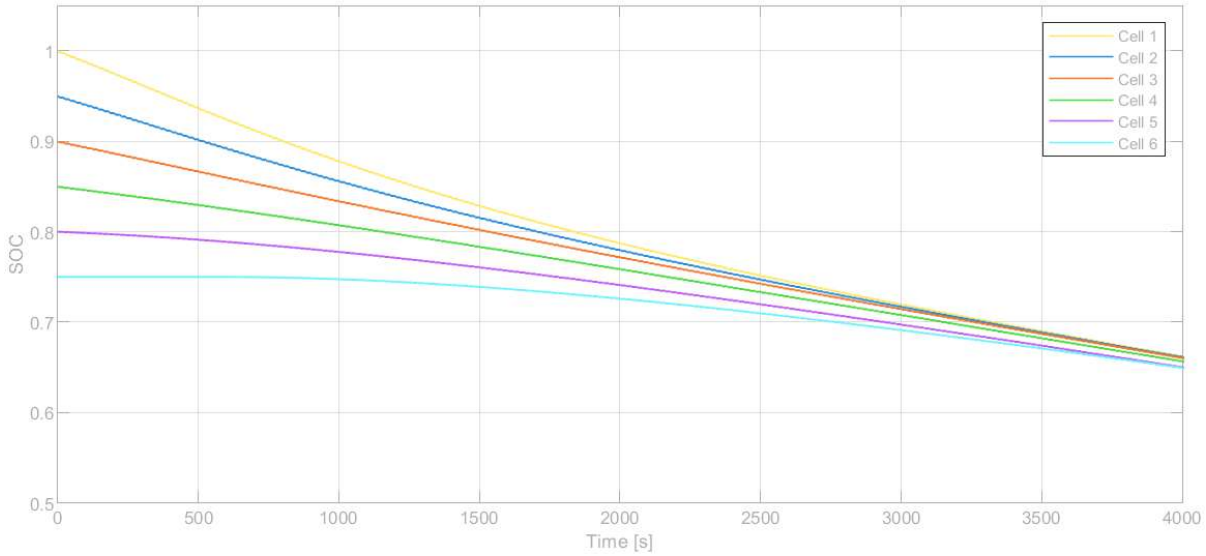

Figure 4.6 SOC.

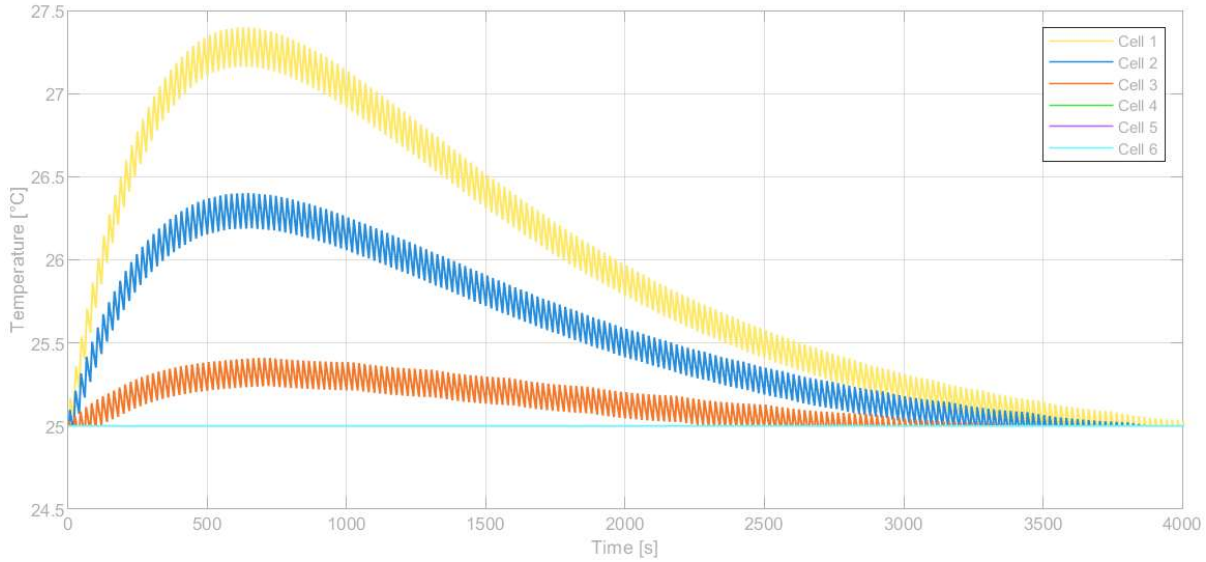

Figure 4.7 Temperature.

Figure 4.4 shows that the current is not uniformly distributed across all cells. Instead, each cell conducts current for different time durations. This enables balancing, as cells with higher SOC and lower temperatures are used more frequently to compensate for the imbalance.

In Figure 4.5, the cell voltages are shown. Initially, the cell with the highest SOC has the highest voltage. This is because the SOC imbalance is reflected in the voltage. The voltage of a battery is influenced by the electrochemical potential of the electrodes. This means that as the cell stores more charge, the potential difference between the electrodes increases, increasing the voltage. Over time, the voltages of all cells converge, which is a result of balancing.

Figure 4.6 shows the SOC. Here, it is seen that over time, the ANN balancing control successfully aligns all SOC values. The cells with the highest initial SOC values are used more until they begin to match the SOC values of the lower ones.

In Figure 4.7, the temperature of the cells are shown. All cells start at the reference temperature, however the cells that are used more frequently also increases moderately in temperature because of higher conduction activity. This is as expected and the temperature rise remains within acceptable limits. This behavior is consistent with the control objective, where SOC balancing is prioritized slightly more than temperature.

From these results, it is evident that the ANN balancing control works efficiently and achieves convergence within a time span of 2500 seconds. The rapid convergence observed highlights the effectiveness of the system in quickly correcting imbalances and stabilizing the battery pack. This result shows the strength of the proposed intelligent balancing approach in managing complex battery dynamics and achieving uniform operation.

4.5 Robustness Simulation

In the previous simulations the load current is modeled as a fixed value. In practical applications the current value is obtained using sensors which are not precise and have accuracy limitations. Current sensors typically have accuracy tolerances ranging from 1% and up to 10% depending on their quality. To investigate the robustness of the ANN balancing control, sensor noise is introduced in the simulation. This is done by adding a band-limited white noise block to the current. This block generates normally distributed random noise which is constrained in bandwidth to simulate the sensor behavior. The power level of this block is chosen assuming the worst case, and thus allowing currents of approximately ±10% of the nominal load current. The load current with simulated sensor noise is seen in Figure 4.8.

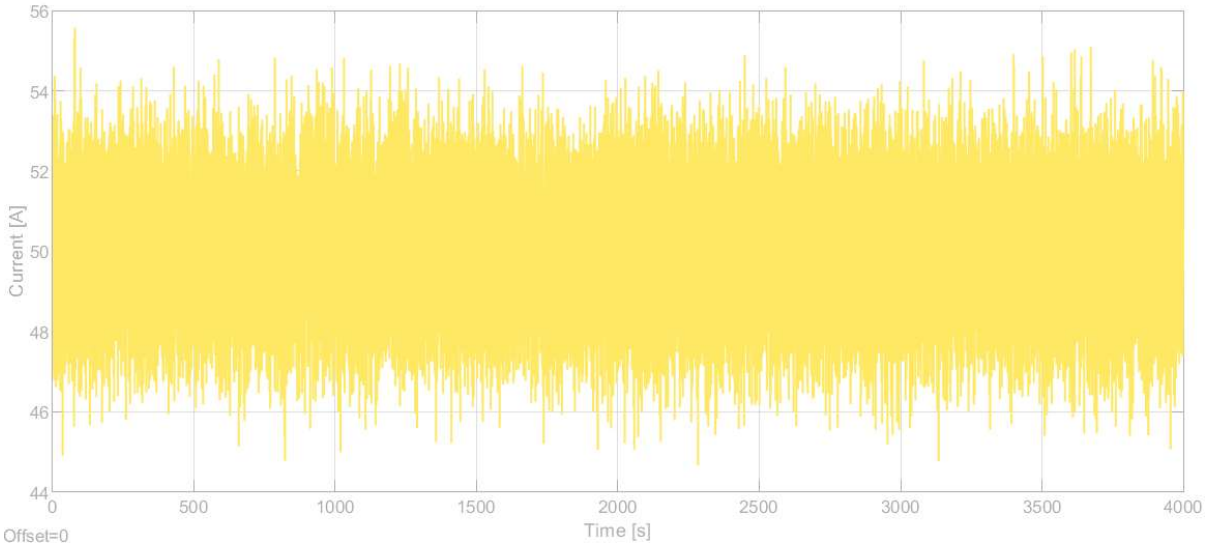

Figure 4.8 Current with noise.

Here, it is seen that the current now contains high frequency noise, which could be caused by sensing. The results of noise on the rest of the system are seen in Figure 4.9 and Figure 4.10.

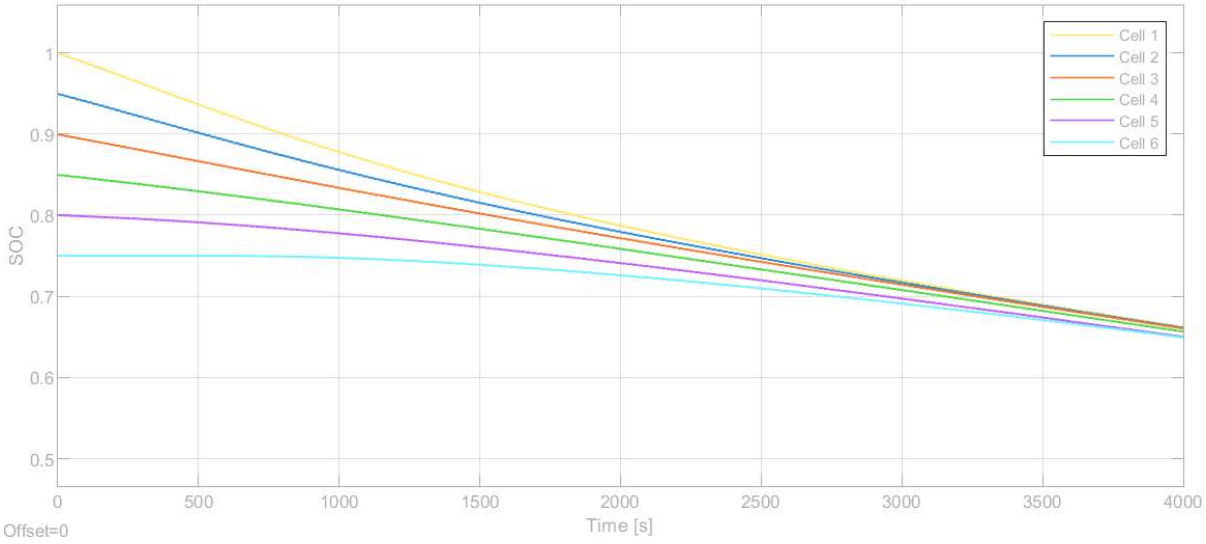

Figure 4.9 SOC with noise.

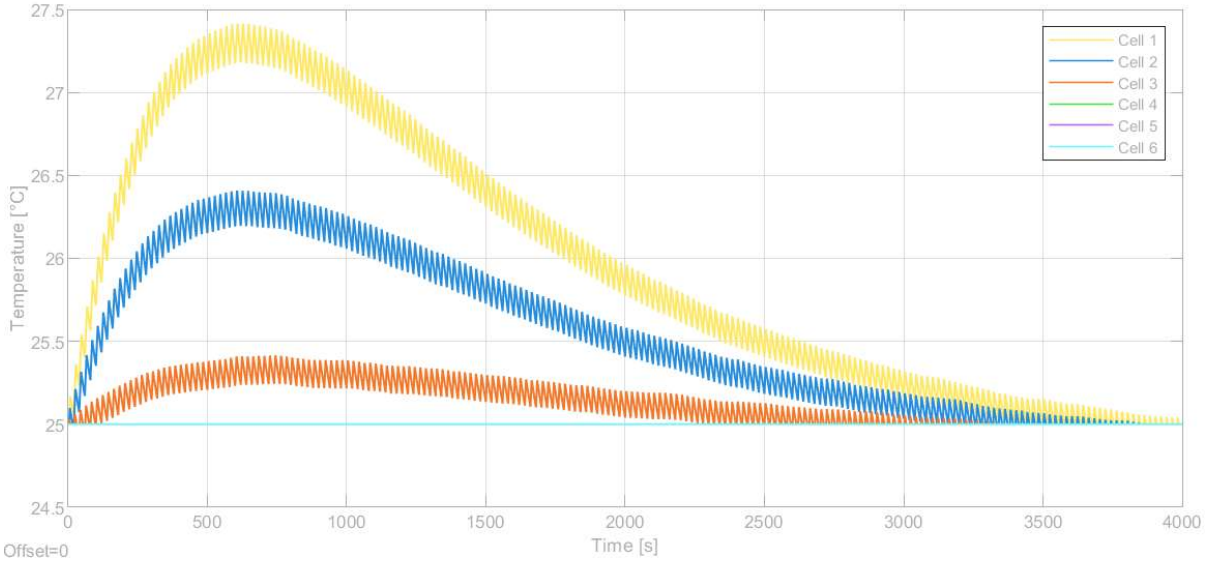

Figure 4.10 Temperature with noise.

It is seen that despite the addition of sensor noise, the ANN balancing control maintains stable and effective operation. In Figure 4.9 it is seen that the SOC still converges within 2500 seconds. Similarly, in Figure 4.10, the same tendencies as without noise is seen. The temperature increases moderately in the most used cells before they converge. These results shows that the ANN control is robust against sensor measurement inaccuracies.

5 Validation of Management System

The testing of control algorithms on modular smart batteries has safety challenges due to the nature of batteries. To ensure a safe environment, a virtual platform is used. This is done by using a Digital Signal Processor (DSP) instead of a battery cell. The aim is to validate the performance of the bypass method without using physical batteries. This setup enables testing under safe conditions and is used as a preliminary step before testing on actual batteries. An overview of the setup is presented in Figure 5.1.[19]

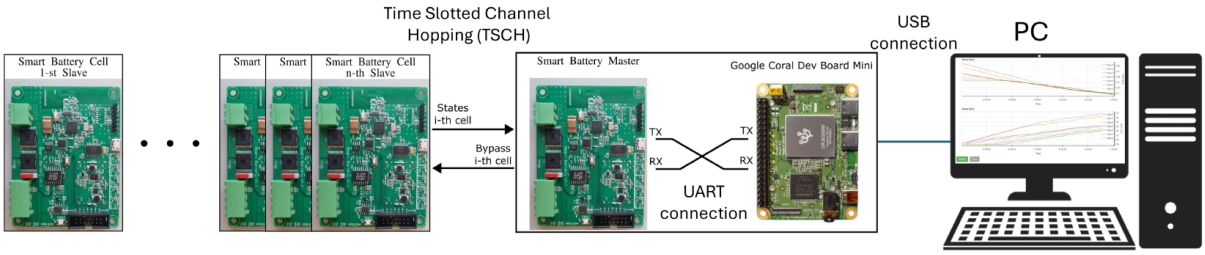

Figure 5.1 Virtual platform overview.[19]

The system consists of eight slave DSPs, each running a simulation of a battery cell. The slave devices are Texas Instruments CC2652R microcontrollers. A master DSP collects information from all the slave units and provides it to the control unit, which is a Google Coral Dev Board Mini. Here, the control algorithm is implemented. Additionally, the Coral board is connected to a PC to monitor the battery system.

The control implemented on the Coral Board is based on a K-Nearest Neighbor (KNN) classification algorithm. It works by connecting or bypassing individual cells to achieve a desired output voltage from the battery pack while simultaneously balancing the SOC across the cells. In general KNN algorithm works by selecting an optimal subset of cells using a given dataset of points and a reference point. The algorithm computes the distance between each point in the dataset and the reference and then selects the K points with the smallest distances to the nearest neighbors. In this case, each cell is represented by its individual SOC. Whereas the reference point is defined by a maximum SOC representing the ideal balancing target. The distance between points is calculated by a weighted Euclidean norm, evaluating the deviation of each cell's SOC from the reference point. The number of selected neighbors K corresponds to the number of cells required to achieve the desired output voltage, which in this test is 6.8 V meaning that two cells should be inline at all times. The functions of all boards are illustrated in Figure 5.2.[19]

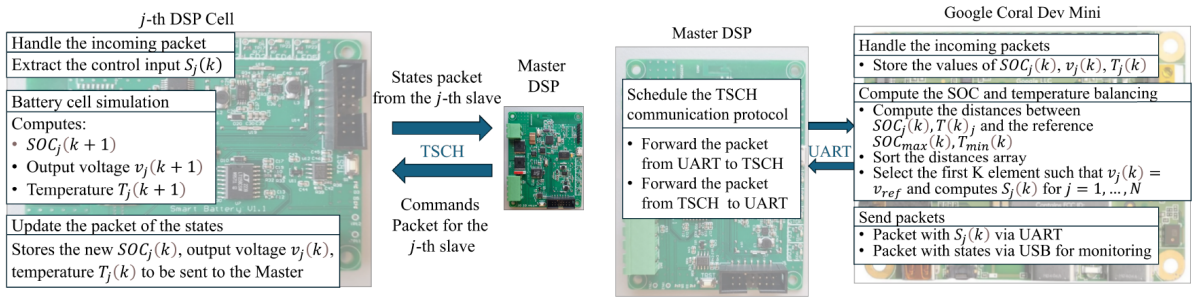

(a) Functions of each DSP cell.

(b) Functions of the control board.

Figure 5.2 Functions of all boards.[19]

The simulated dynamic behavior of each battery cell is then visualized to better validate the performance of the control. Here, the key parameters are the slave voltage, current and SOC. The results of the test is seen in Figure 5.3.

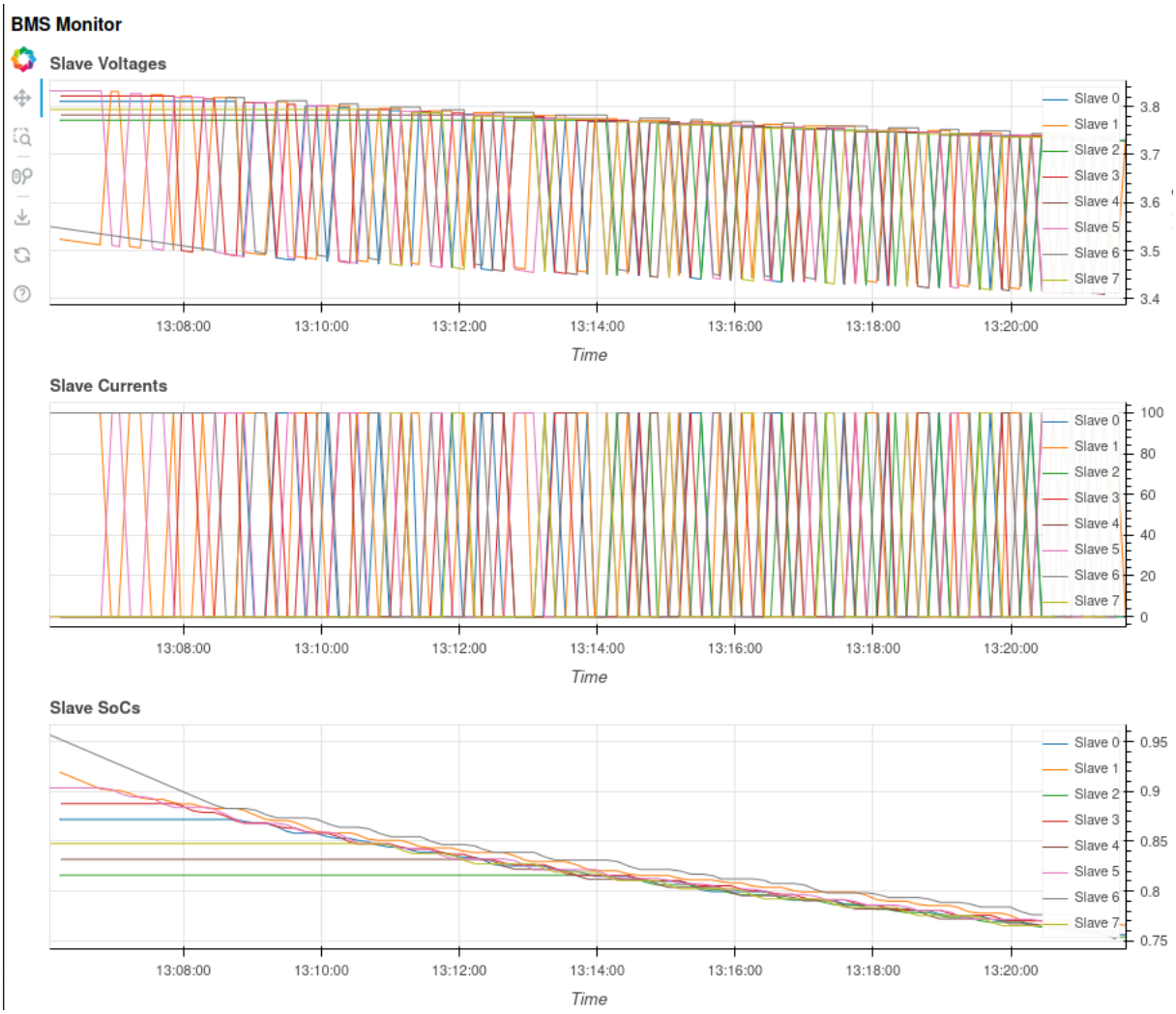

Figure 5.3 Results of virtual platform test.

These results shows that SOC balancing is achieved among the simulated battery cells. Cells are dynamically inline or bypassed based on their individual SOC levels. This means that the bypass method operates as intended and enables selective usage of cells to ensure uniform SOC. This will in turn increase the performance of the battery pack. Furthermore, it shows that the virtual platform can be used to validate the control of modular smart battery systems without involving real battery cells.

6 Discussion

This chapter discusses the results presented in this project. The analysis includes an investigation of the limitations in the model, control and validation.

6.1 Use of Equivalent Circuit Model

The ECM is a simple and computationally efficient way of simulating the behavior of a battery. This comes at a cost due to its limitations in accuracy. ECMs simplify the electrochemical processes inside a lithium-ion cell and may not capture the degradation effects or nonlinear dynamics under varying load conditions. This could lead to inaccuracies in SOC and temperature estimation. These inaccuracies will then affect the performance of the ANN balancing control, as it relies on accurate input signals to make optimal switching decisions. This could affect the efficiency of the BMS.

6.2 Simplified SOC Estimation

The SOC estimation is based on the Coulomb counting method. It integrates the current over time in order to estimate the charge flow of the battery. While this approach is commonly used due to its simplicity it is sensitive to measurement drift and sensor inaccuracies. Over time small errors in current sensing or integration can lead to deviations in the estimated SOC. The accuracy could be improved by including a correction technique.

6.3 Validation of ANN Control

Although the ANN control performed well in simulation, it is not implemented on the Coral Dev Board in this project. As a result, the ANN control strategy is not validated. Deployment to the Coral platform is essential to verify its responsiveness under discrete constraints.

6.4 Ideal Switching

In the simulations it is assumed that the switching behavior is ideal. In practical applications there is always a delay between turn ON and turn OFF of a switching device. Transistors have rise and fall times when going from a state of conducting to a state of blocking the current. In this case, dead time might be needed to ensure that a battery cell is not shorted. By adding dead time, it might increase the time before convergence of SOC and temperature is achieved which will affect the overall efficiency of the BMS.

6.5 Validation using Real Batteries

While the virtual platform is useful for testing control safely, testing on real batteries should be done in order to fully validate the balancing methods. This is due to the limitations of the virtual platform, which are the lack of electrical parasitics and real switching transients. These effects can affect the switching behavior, introduce noise or voltage spikes. Without investigating the effect of these, the control performance may seem ideal in simulation but degrade under physical conditions. Therefore, hardware testing is essential to ensure the robustness, efficiency, and safety of the proposed balancing system in practical applications.

7 Conclusion

This project successfully develops a BMS, which is able to balance both SOC and temperature in a modular smart battery pack. The project made digital models of a battery cell and the battery pack, which includes dynamic behaviors, cell connections, and bypass switches. The switches are successfully controlled by PWM signals generated from ANN outputs. ANN made effective switching decisions based on inputs of cell SOC and temperature. Here, the simulation results shows that the SOC and temperature converged within 2500 seconds.

To investigate the robustness of the system, a noise simulation is conducted by introducing sensor inaccuracy into the measured current signal. Despite $\pm 10\%$ fluctuations from added white noise, the ANN control strategy maintains a stable performance, successfully converging the SOC of all cells within the same 2500 seconds. This result confirms the resilience of the balancing method under more realistic sensing conditions.

Furthermore, the virtual prototyping platform enables safe validation of the balancing method without using real battery hardware. This provides the possibility of implementing and testing the ANN control algorithm in an safe environment.

These results highlight the potential of using power electronic switches and BMS to improve battery performance, longevity, and efficiency in electric vehicle applications.

8 Future Work

To build upon the results of this project, several key steps are proposed for future work.

The first step is to validate the ANN control algorithm using the virtual platform. To do this, the ANN control should be programmed on the coral board. This would then allow the ANN control to be tested under more realistic conditions without involving physical battery cells, which ensures a safe environment for analyzing performance and improvement.

Once validated using the virtual platform, the next step would involve developing the necessary hardware for the BMS method. This includes making the actual switching circuit. Here, Metal-Oxide-Semiconductor Field-Effect Transistor (MOSFET)s could be considered due to their high efficiency, fast switching capabilities, and compatibility with digital control signals. Testing on hardware will allow analysis of the ANN control with actual switching devices needed to validate the control performance when non-ideal switches are included.

The last step would then be to test the complete BMS. This includes the ANN control and switching hardware. It should be tested on real battery cells. This step validates the system's performance under real electrical, thermal and dynamic conditions.

Bibliography

[1] European Commission, "The european green deal," 2020. [Online]. Available: https://commission.europa.eu/strategy-and-policy/priorities-2019-2024/european-green-deal_en

[2] International Energy Agency, "Road transport," 2023. [Online]. Available: https://www.iea.org/reports/road-transport

[3] ——, "Global ev outlook 2024," 2024. [Online]. Available: https://www.iea.org/reports/global-ev-outlook-2024

[4] J. W. Choi and D. Aurbach, "Promise and reality of post-lithium-ion batteries with high energy densities." *Nature Reviews Materials*, 2016.

[5] Q. Ouyang, R. Ma, Z. Wu, and Z. Wang, "Optimal fast charging control for lithium-ion batteries," *IFAC-PapersOnLine*, 2020.

[6] Z. Liu, Y. Yang, K. Wang, Z. Shao, and J. Zhang, "Post: Parallel offloading of splittable tasks in heterogeneous fog networks," *IEEE Internet of Things Journal*, 2020.

[7] S. Ouyang, Y. Li, X. Wu, Y. Wang, F. Liu, J. Zhang, Y. Qiu, Z. Zhou, Z. Wang, W. Xia, and X. Lin, "Gpr4 signaling is essential for the promotion of acid-mediated angiogenic capacity of endothelial progenitor cells by activating stat3/vegfa pathway in patients with coronary artery disease," *Stem Cell Research and Therapy*, 2021.

[8] M. Waseem, M. Ahmad, A. Parveen, and M. Suhaib, "Battery technologies and functionality of battery management system for evs: Current status, key challenges, and future prospectives," *Journal of Power Sources*, 2023.

[9] Y. Qin, S. Adams, and C. Yuen, "Transfer learning-based state of charge estimation for lithium-ion battery at varying ambient temperatures," *IEEE Transactions on Industrial Informatics*, 2021.

[10] C. Vidal, P. Malysz, P. Kollmeyer, and A. Emadi, "Machine learning applied to electrified vehicle battery state of charge and state of health estimation: State-of-the-art," *IEEE Access*, 2020.

[11] H. Sorouri, A. Oshnoei, Y. Che, and R. Teodorescu, "A comprehensive review of hybrid battery state of charge estimation: Exploring physics-aware ai-based approaches," *Journal of Energy Storage*, 2024.

[12] A. Kulkarni, A. Nadeem, R. Di Fonso, Y. Zheng, and R. Teodorescu, "Novel low-complexity model development for li-ion cells using online impedance measurement," *Journal of Energy Storage*, 2024.

[13] H. Sorouri, A. Oshnoei, and R. Teodorescu, "Intelligent cell balancing control for lithium-ion battery packs," in *2024 IEEE 10th International Power Electronics and Motion Control Conference, IPEMC 2024 ECCE Asia*, 2024.

[14] D. Bernardi, E. Pawlikowski, and J. Newman, "A general energy balance for battery systems," *Lawrence Berkeley National Laboratory Publications*, 1984. [Online]. Available: https://escholarship.org/uc/item/9fx5f0h8

[15] A. Kulkarni, H. Sorouri, Y. Zheng, X. Sui, A. Oshnoei, N. A. Weinreich, and R. Teodorescu, "Li-ion battery digital twin based on online impedance estimation," in *2023 IEEE 17th International Conference on Compatibility, Power Electronics and Power Engineering (CPE-POWERENG)*, 2023.

[16] H. Sorouri, A. Oshnoei, A. Safari, P. Davari, M. Zacho, A. Johnsen, and R. Teodorescu, "Accelerated soh balancing in lithium-ion battery packs using finite set mpc," in *Aalborg University's Research Portal*, 2025.

[17] H. Sorouri, A. Oshnoei, and R. Teodorescu, "Intelligent cell balancing control for lithium-ion battery packs," in *2024 IEEE 10th International Power Electronics and Motion Control Conference (IPEMC2024-ECCE Asia)*, 2024.

[18] ——, "Intelligent dual balancing of soc and temperature in lithium-ion battery packs using brain emotional learning," in *Aalborg University's Research Portal*, 2025.

[19] R. Teodorescu, D.-I. Stroe, X. Sui, N. A. Weinreich, Y. Che, A. Kulkarni, Y. Zheng, S. B. Vilsen, P. Bharadwaj, M. D. Christensen, and B. Steffensen. Smart battery. [Online]. Available: https://vbn.aau.dk/en/projects/smart-battery

A Simulink Model overview

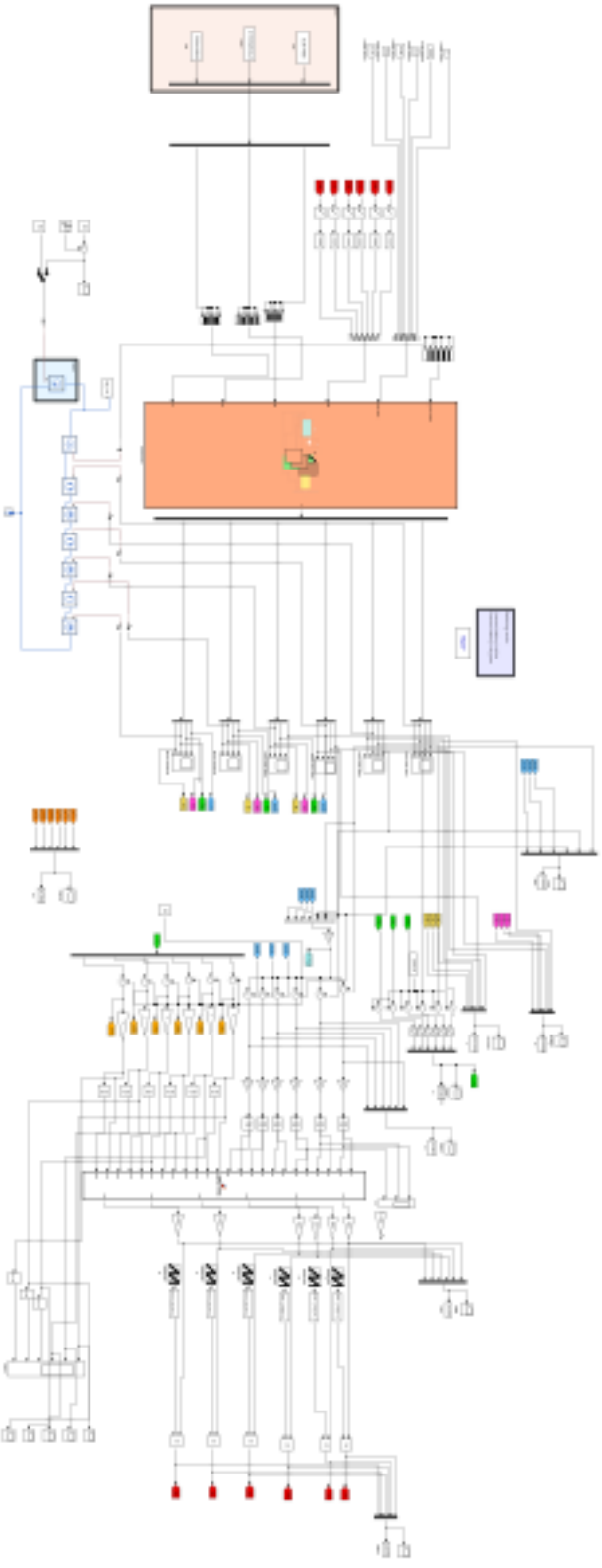

B Battery Cell Model

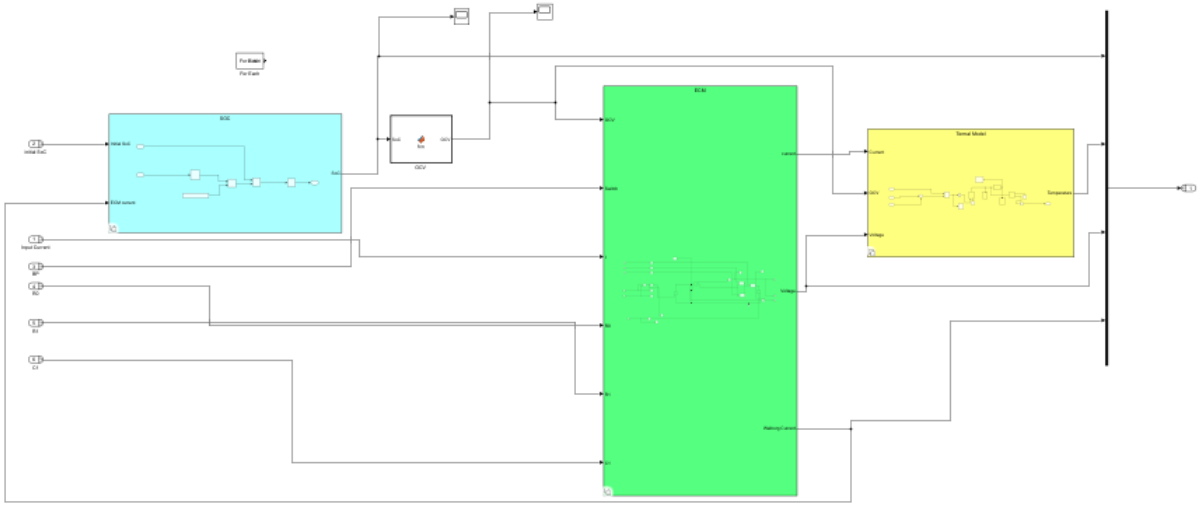

Figure B.0.1 Overview of battery cell model in Simulink.

B.1 SOC Estimation

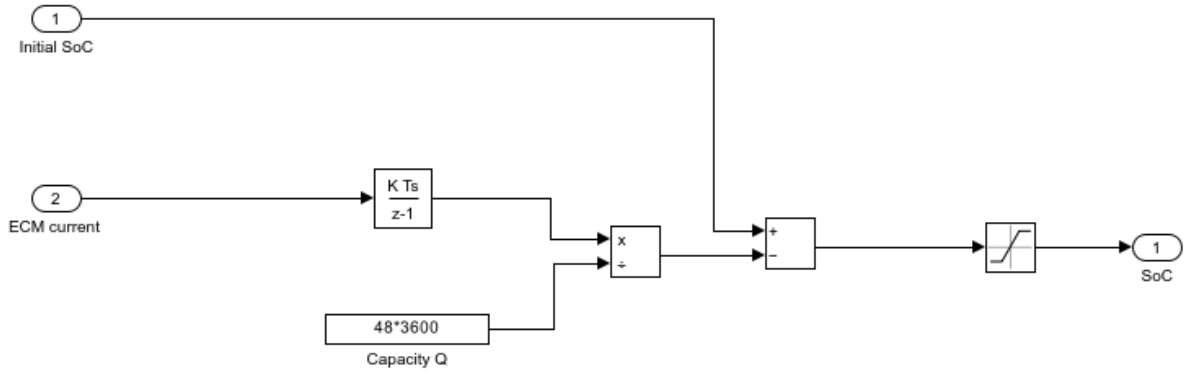

Figure B.1.1 SOC estimation in Simulink.

B.2 OCV Estimation

```
1  function OCV = fcn(SOC)
2  x=SOC;
3  p1  = 2.178780551152078e+03;
4  p2  = -1.059911178403064e+04;
5  p3  = 2.181082635032735e+04;
6  p4  = -2.467974815466170e+04;
7  p5  = 1.671355603708102e+04;
8  p6  = -6.915835559409158e+03;
9  p7  = 1.717673711564352e+03;
10 p8  = -2.430223804179180e+02;
11 p9  = 18.246620866965540;
12 p10 = 2.948413921752475-0.022;
13 OCV = p1*x^9 + p2*x^8 + p3*x^7 + p4*x^6 + p5*x^5 + p6*x^4 + p7*x^3 + p8*x^2 + p9*x +
       p10;
14 end
```

B.3 ECM

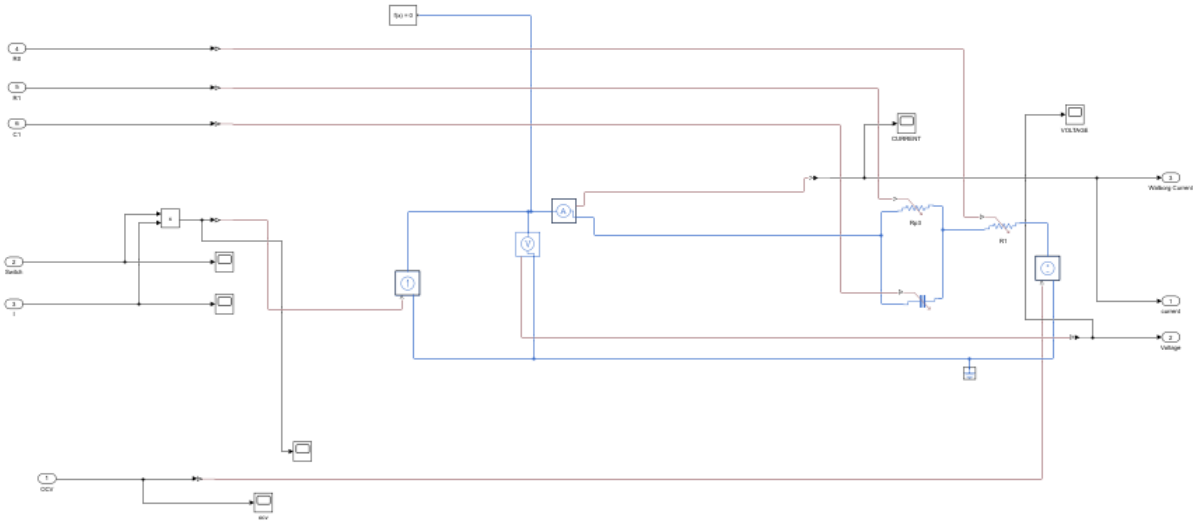

Figure B.3.1 ECM in Simulink.

B.4 Thermal Model

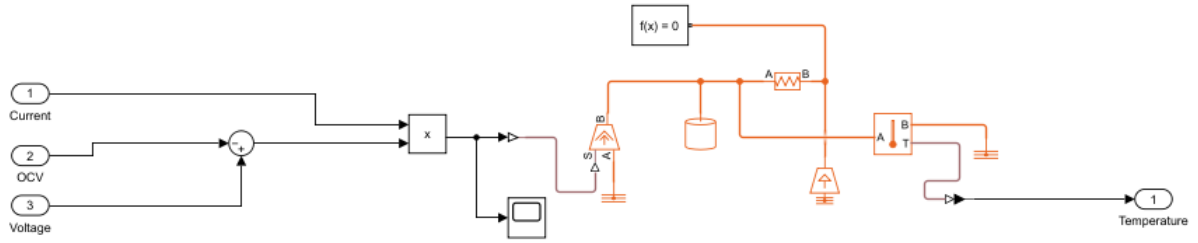

Figure B.4.1 Thermal model in Simulink

C ANN Control Function

```
function [k1, k2 ,k3,k4, k5, k6]=

ANN_Tuner(e1,d1,e2,d2,e3,d3,e4,d4,e5,d5,e6,d6,eT1,dT1,eT2,dT2,eT3,dT3,eT4,dT4,eT5,dT5,
    eT6,dT6)

numberinput=9;
neuronlayerone=50;
neuronlayertwo=24;
eta=0.2;

X=2*ones(numberinput,1);
w1old=ones(neuronlayerone,numberinput);
w2old=ones(neuronlayertwo,neuronlayerone);
deltaw1=zeros(size(w1old));
deltaw2=zeros(size(w2old));

for iteration=1:5
    w1new=w1old+deltaw1;
    w2new=w2old+deltaw2;
    w1old=w1new;
    w2old=w2new;
    net1=w1new*X;
    h=1./(1.+(exp(1)).^(-net1));
    net2=w2new*h;
    delta=[d1;e1;eT1;dT1;d2;e2;eT2;dT2;d3;e3;eT3;dT3;d4;e4;eT4;dT4;d5;e5;eT5;dT5;d6;e6;
    eT6;dT6];%*(derive2);%.*derive;
    deltaw2=eta*delta*h';
    sigmaj=(h.*(1-h)).*((w2new)'*delta);
    deltaw1=eta*sigmaj*X';
end

k1=0.5*(0.9*net2(2)-0.2*net2(3));
k2=0.5*(0.9*net2(6)-0.2*net2(7));
k3=0.5*(0.9*net2(10)-0.2*net2(11));
k4=0.5*(0.9*net2(14)-0.2*net2(15));
k5=0.5*(0.9*net2(18)-0.2*net2(19));
k6=0.5*(0.9*net2(22)-0.25*net2(23));

end
```